Visual Neuroscience (1993), **10**, 1081–1098. Printed in the USA.

Morphology of a small-field bistratified ganglion cell type in the macaque and human retina

DENNIS M. DACEY

Department of Biological Structure, University of Washington, Seattle

(RECEIVED February 1, 1993; ACCEPTED March 31, 1993)

Abstract

In *in-vitro* preparations of both macaque and human retina, intracellular injections of Neurobiotin and horseradish peroxidase were used to characterize the morphology, depth of stratification, and mosaic organization of a type of bistratified ganglion cell. This cell type, here called the small bistratified cell, has been shown to project to the parvocellular layers of the dorsal lateral geniculate nucleus (Rodieck, 1991) and is therefore likely to show color-opponent response properties.

In both human and macaque, the two dendritic tiers of the bistratified cell are narrowly stratified close to the inner and outer borders of the inner plexiform layer. The inner tier is larger in diameter and more densely branched than the outer tier and gives rise to distinct spine-like branchlets bearing large, often lobulated heads. By contrast the smaller, outer tier is sparsely branched and relatively spine-free.

In human retina, the small bistratified cells range in dendritic field diameter from ~50 μm in central retina to ~400 μm in the far periphery. The human small bistratified cells are about 20% larger in dendritic-field diameter than their counterparts in the macaque. However, when the difference in retinal magnification between human and macaque is taken into account, the small bistratified cells are similar in size in both species. In macaque, the small bistratified cell has a dendritic-field size that is ~10% larger than that of the magnocellular-projecting parasol ganglion cell. Human small bistratified ganglion cells tend to have smaller dendritic-field diameters than parasol cells. This is because parasol ganglion cells are larger in human than in macaque retina (Dacey & Petersen, 1992).

In macaque retina, intracellular injections of Neurobiotin revealed heterotypic tracer coupling to a distinct mosaic of amacrine cells and probable homotypic coupling to an array of neighboring ganglion cells around the perimeter of the injected cell's dendritic tree. The amacrine cell mosaic had a density of 1700 cells/mm^2 in peripheral retina. Individual amacrines had small, densely branched and bistratified dendritic fields. From the homotypic coupling, it was possible to estimate for the small bistratified cell a coverage factor of ~1.8, and a density of ~1% of the total ganglion cells in central retina, increasing to ~6–10% in the retinal periphery.

The estimated density, dendritic-field size, and depth of stratification all suggest that the small bistratified ganglion cell type is the morphological counterpart of the common short-wavelength sensitive or 'blue-ON' physiological type.

Keywords: Macaque retina, Human retina, Color opponent, Ganglion cell types, Parvocellular pathway, Blue-cone pathway

Introduction

In macaque monkey, the parvocellular layers of the lateral geniculate nucleus receive input from two major groups of color-opponent retinal ganglion cells: those that receive antagonistic input from medium- and long-wavelength-sensitive (M- and L-) cones, the red-green cells, and those that receive input from short-wavelength-sensitive (S-) cones opposed by a combination of M- and L-cone input, the blue-yellow cells (Wiesel & Hubel, 1966; De Valois et al., 1967; de Monasterio & Gouras, 1975; Dreher et al., 1976; Creutzfeldt et al., 1979; Derrington et al., 1984). In an early attempt to identify the morphology of the red-green and blue-yellow cells by employing intracellular recording and dye injection, it was concluded that ganglion cells receiving blue-cone input were morphologically distinct from those that receive red-green cone input (de Monasterio, 1979). The blue-ON cells appeared to have larger cell bodies and larger dendritic fields than the red-green cells and de Monasterio suggested that they corresponded to the parasol ganglion cell type originally described by Polyak (1941). Recent results argue against this suggestion since it has been shown that the great majority of axons projecting to the parvocellular layers arise from the midget or P-beta ganglion cells and that the parasol, or P-alpha cells, project to the magnocellular layers (Perry et al., 1984), where phasic, non-opponent cells are recorded.

Reprint requests to: Dennis Dacey, Department of Biological Structure, SM-20, University of Washington, Seattle, WA 98195, USA.

The two classes of color-opponent cells would therefore appear to be contained within the midget ganglion cell population.

A new line of evidence has renewed support for the possibility that the two different color-opponent pathways may originate from separate ganglion cell populations that project in parallel to the parvocellular layers of the lateral geniculate nucleus (Rodieck & Watanabe, 1988; Rodieck, 1991). The evidence comes from experiments in which intracellular injections of horseradish peroxidase were used to reveal the morphology of ganglion cells that had been retrogradely labeled from central injection sites. The results showed that ganglion cell types other than the parasol and midget cells project to the lateral geniculate nucleus in macaque. These less-common ganglion cell types have not yet been characterized in detail and their functional significance remains a matter of speculation, but the existence of parvocellular projecting ganglion cell types beyond the midget cells provides some support for the assertion that more than one ganglion cell type conveys spectral information to the lateral geniculate nucleus.

One group of non-midget ganglion cells that project to the parvocellular layers shows a bistratified dendritic morphology (Rodieck, 1991). Rodieck argued that these bistratified cells could give rise to an important non-midget cell red-green and blue-yellow opponent pathway with all of the properties necessary for color perception. In the present study, this hypothesis was evaluated further by attempting to identify and characterize the morphology of the bistratified cell type in more detail. One important question is whether the bistratified ganglion cells represent a single cell type or multiple cell types. A second question is whether the depth of stratification of the dendritic tree could provide any insight into the bipolar inputs to these cells. It was possible to reliably recognize these ganglion cells, called here the small bistratified cells, using intracellular injection techniques in both the macaque and human retina. Analysis of the dendritic morphology, dendritic-field size, spatial density, and depth of dendritic stratification of the small bistratified ganglion cells shows that they comprise a single morphologically distinct cell type. The depth of stratification of the small bistratified cell suggests that it could receive direct input from the blue-cone bipolar cell (Kuoyama & Marshak, 1992), and correspond to the most common ganglion cell in the blue-yellow color-opponent class: the blue-ON cell.

Material and methods

In vitro isolated retina

The retinal preparation and the intracellular injection technique for both the macaque and human retina have been described previously (Dacey, 1989; Dacey & Petersen, 1992). Eyes from *Macaca nemestrina* (n = 21) were obtained from the tissue distribution program of the Regional Primate Center at the Uni-

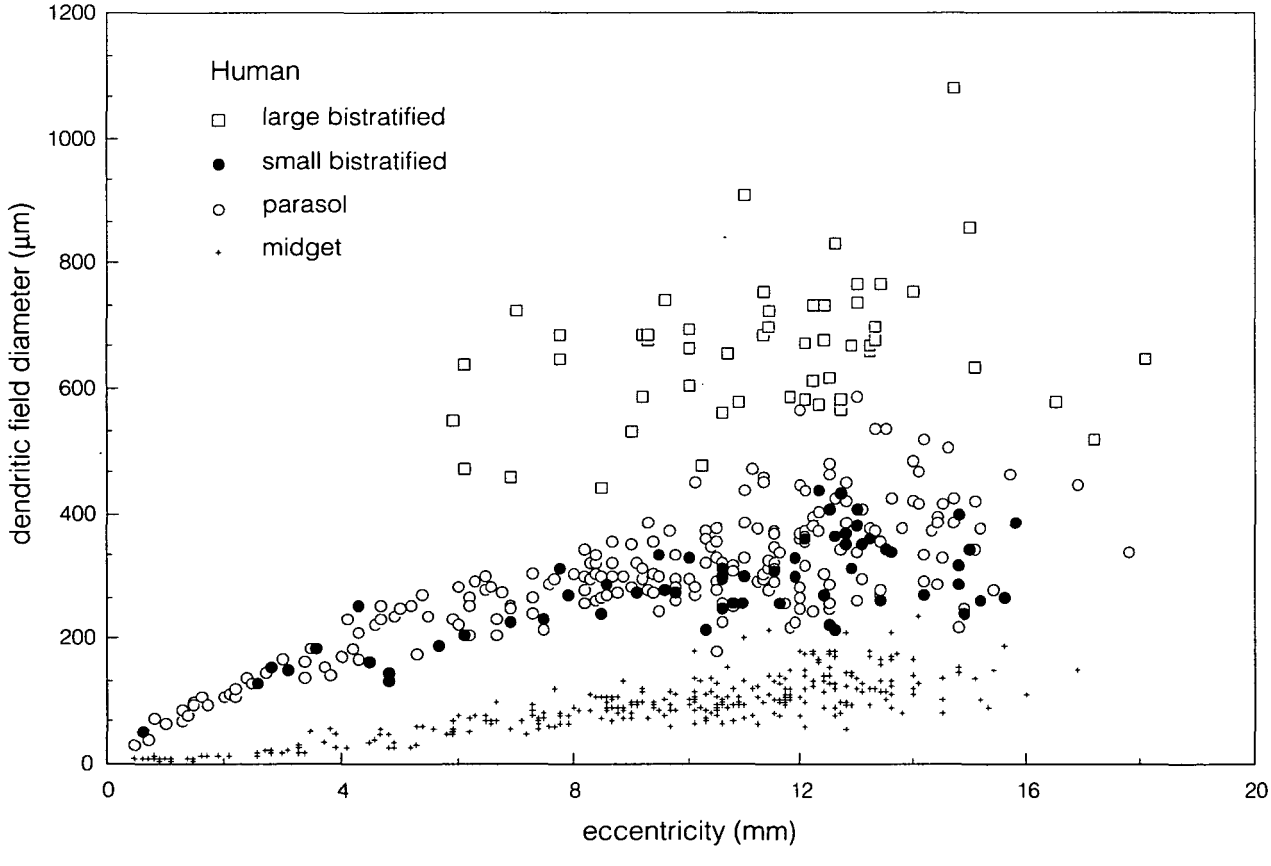

Fig. 1. Dendritic-field diameters of human midget, parasol, and bistratified ganglion cells plotted as a function of eccentricity. Cells designated as small bistratified ganglion cells (filled circles) overlap the parasol cells (unfilled circles) in dendritic-field size. The cells designated as large bistratified cells (squares) comprise a number of morphologically distinct types that, at a given retinal eccentricity, are larger in diameter than either the parasol or the small bistratified ganglion cells.

versity of Washington immediately after animals were euthanized. Human eyes ($n = 46$; age range 16–82 years) were obtained 90–120 min after death from donors to the Lions Eye Bank at the University of Washington. In both human and macaque, the retina was dissected by cutting the eye with a razor blade at the corneoscleral junction and draining the vitreous humor from the eyecup. In most instances, the vitreous humor could be poured from the eyecup with no adherence to the retina; in some cases, however, particularly in eyes donated from young adults, the vitreous humor was more tenacious and brief pressure on the eye at the junction of the sclera and the optic nerve was required to break any attachments to the retina before the vitreous humor could be drained from the eyecup. Complete removal of the vitreous humor was necessary for survival of the retina *in vitro*. After removal of the vitreous humor, the eye was placed in a continuously oxygenated tissue-culture medium (Ames, Sigma Chemical Co., St. Louis, MO) and the retina was dissected free of the sclera and choroid and then freed from the eyecup by cutting the optic nerve head. Each retina was maintained in the chamber for ~8–10 h with no apparent deterioration in cellular morphology. At the end of an experiment, the retina was removed from the chamber and fixed for 2–3 h in a phosphate-buffered fixative (2% glutaraldehyde/2% paraformaldehyde or 4% paraformaldehyde; 0.1 M, pH 7.4).

Intracellular injection and histology

Retinal cells were stained *in vitro* with the fluorescent dye, acridine orange, and observed under blue episcopic illumination. Intracellular injections were made into the fluorescing cells under direct microscopic control with beveled, microcapillary glass electrodes made with a Brown-Flaming electrode puller (P-87, Sutter Instruments, San Rafael, CA) and beveler. Electrodes were filled with a solution of Lucifer Yellow (~2%; Aldrich Chemical, Milwaukee, WI) in 20 mM, pH 7.0 MOPS buffer (Sigma Chemical Co., St. Louis, MO) and either rhodamine-conjugated horseradish peroxidase (HRP) (~4%; Sigma Chemical Co., St. Louis, MO) or Neurobiotin (~4%; Vector Labs, Burlingame, CA). HRP-filled electrodes were beveled to a resistance of ~40 MΩ. Neurobiotin-filled electrodes were beveled to a resistance of ~80 MΩ or left unbeveled (~120 MΩ). Lucifer Yellow fluorescence in the electrode and the acridine-orange fluorescence of the ganglion cells were observed with the same excitation filter (410–490 nm; barrier filter 51 nm), permitting direct observation of the electrode tip as it penetrated a cell. Lucifer Yellow was passed into an impaled cell with 1–2 nA negative current for 30 s to confirm a successful penetration and to identify the cell type being injected or its depth of stratification in the inner plexiform layer (IPL). Rhodamine-conjugated HRP was subsequently passed into the cell with 1–5 nA positive current for 1–3 min and was observed directly with a green filter (excitation filter 545 nm long pass; barrier filter 590 nm). Neurobiotin was injected with 0.1–0.5 nA positive current for 30–60 s but, as it was not conjugated to a fluorescent tag, it could not be observed passing into the cell.

For the cells that were injected with rhodamine-conjugated HRP, the HRP was demonstrated using DAB as the chromagen. Retinas were incubated in the DAB solution (0.1% in 0.1 M phosphate buffer, pH 7.4) for 5 min. H_2O_2 (0.003%) was then added to the DAB solution and the retinas were further incubated for 3–4 min. Retinas were rinsed in buffer, wholemounted on gelatin coated slides, and air dried for a few hours. The tissue was then dehydrated in a graded alcohol series, cleared in xylene, and coverslipped. When the retina was mounted in this way there was little shrinkage in the plane of the retina (~2%). Radial shrinkage was ~60%; the IPL, for example, was reduced from ~25–30 μm thickness (measurements taken from *in vitro*, acridine-stained retinas) to about ~10–12 μm after dehydration.

The injected Neurobiotin was revealed by a horseradish peroxidase (HRP) reaction product using the Vector ABC protocol (Vector, Elite kit). Retinas fixed in 4% paraformaldehyde were first placed in 0.5% tritonX-100 (in 0.1 M phosphate buffer, pH 7.4) at room temperature for 3 h, and then incubated in buffer containing the Vector avidin-biotin-HRP complex for 3 h. The tissue was then rinsed in buffer for 1 h and

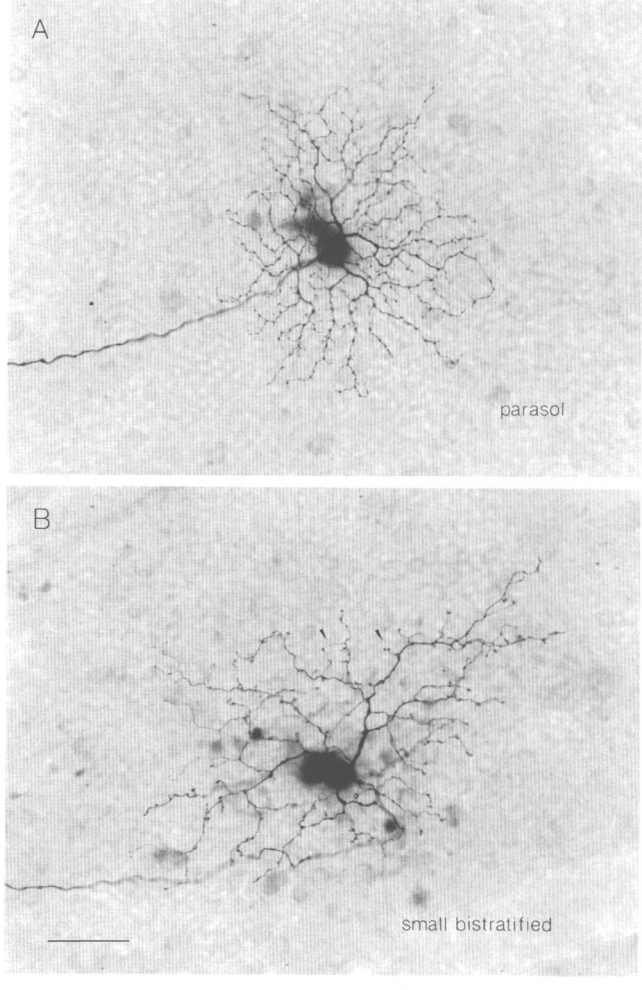

Fig. 2. Photomicrographs of intracellular Neurobiotin-fills of a parasol cell (A) and a small bistratified ganglion cell (B) in the macaque retina (*Macaca nemestrina*). Both cells are from the same retina at 11 mm eccentricity. The cells were separated by about 300 μm. The plane of focus for the small bistratified cell is on the inner dendritic tree, close to the ganglion cell layer. The inner dendritic tree of the small bistratified cell is slightly larger and more sparsely branched than the dendritic field of the parasol cell. Note also that the dendrites of the small bistratified cell give rise to distinct spine-like branchlets with long necks and large, often lobulated heads (two of these dendritic specializations are indicated by the arrowheads in B; the parasol cell, by contrast, shows an abundance of small simple spines). Scale bar = 50 μm.

standard HRP histochemistry was performed using DAB as the substrate, as described above for the HRP reaction. Triton-treated retinas were easily damaged by dehydration and were therefore wholemounted in an aqueous solution of glycerol and polyvinyl alcohol (Heimer & Taylor, 1974). The mountant partially dries to a water-retaining, rubbery film that provides reasonable tissue clarity and permits long-term storage and analysis of the retinas with little or no shrinkage.

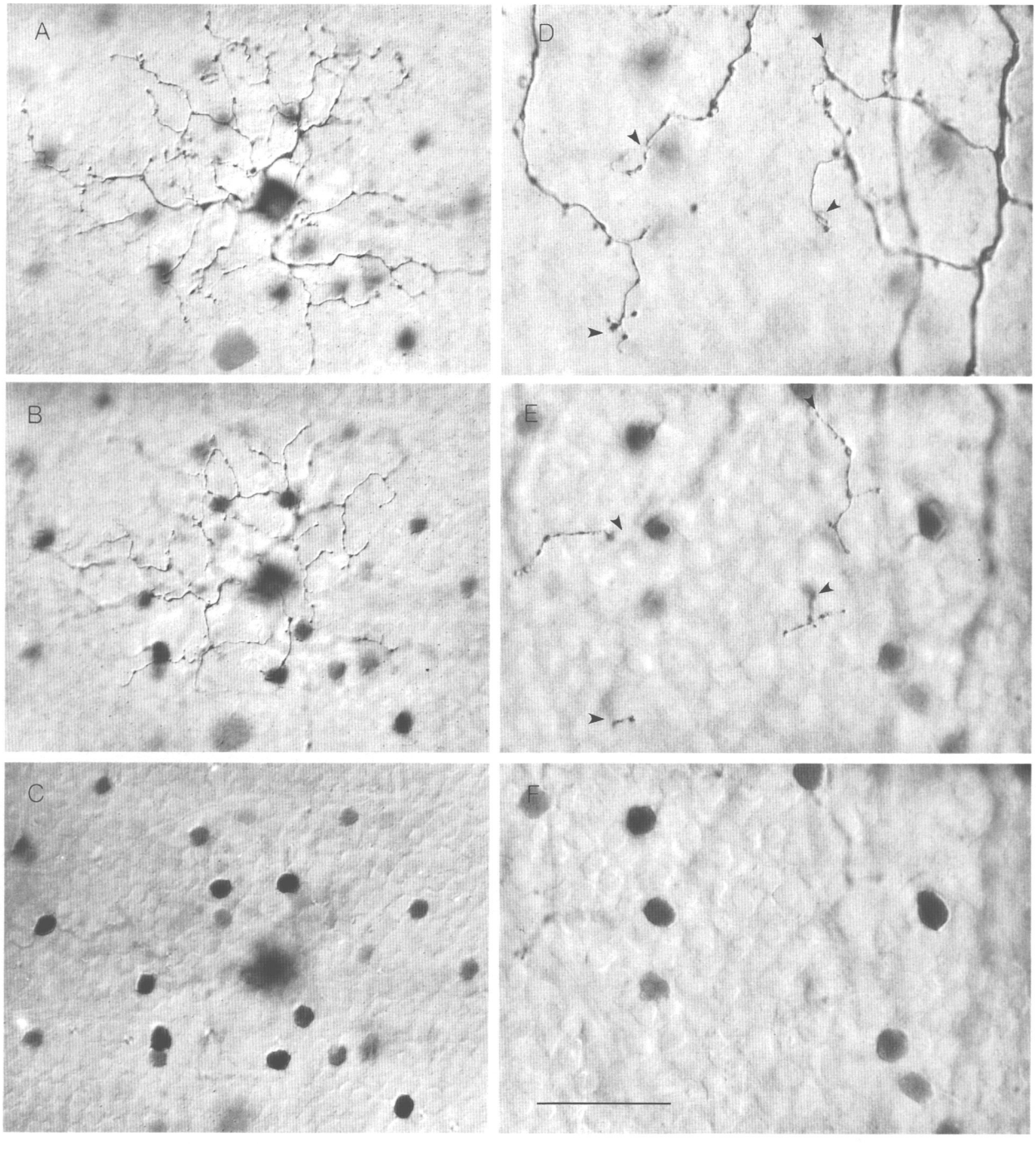

Fig. 3. Photomicrographs of the inner and outer dendritic trees of the small bistratified cell at low (A-C) and high magnification (D-F). A: Plane of focus is on the inner dendritic tier, close to the ganglion cell layer. B: Plane of focus is shifted to the outer dendritic tier close to the inner nuclear layer. The outer tier of dendrites forms a more sparsely branching and smaller diameter tree than the inner tier. C: Plane of focus in the amacrine cell layer shows tracer coupling to a population of amacrine cells whose somata appear darkly stained. D: Higher magnification of the inner dendritic tree of another cell; plane of focus very close to ganglion cell layer. Arrowheads indicate the points of origin of branches that extend to the outer dendritic tree. E: Plane of focus is shifted to the outer tree very close to the inner nuclear layer; note thin, sparse branches compared to the inner tree. F: Plane of focus in the amacrine cell layer. Scale bar for A-C = 50 μm; and D-F = 25 μm.

Conversion to angular eccentricity in degrees

To convert distance from the fovea in millimeters to degrees of visual angle, the nonlinear conversion of Drasdo and Fowler (1974) was used. In this schematic human eye, the distance-to-angle conversion is 275 μm/deg in the fovea and decreases to ~135 μm/deg at 90-deg eccentricity. The nonlinear relationship between retinal distance and visual angle (Fig. 2 in Drasdo & Fowler, 1974) is well fit by the second-order polynomial equation, $y = 0.1 + 3.4x + 0.035x^2$ ($R = 1.0$), where y = eccentricity in degrees and x = eccentricity in millimeters. For the smaller eye of the macaque, the distance-to-angle conversion reported by Perry and Cowey was used (Perry & Cowey, 1985). These authors found a foveal conversion of 223 μm/deg that declined to ~170 μm/deg in the far retinal periphery. The nonlinear relationship between retinal distance and visual angle is well fit by the second-order polynomial equation, $y = 0.1 + 4.21x + 0.038x^2$ ($R = 1.0$).

Data analysis

For each retina, the location of every injected ganglion cell relative to the foveal center was recorded. Each cell was photographed and a simple, camera-lucida tracing of the dendritic

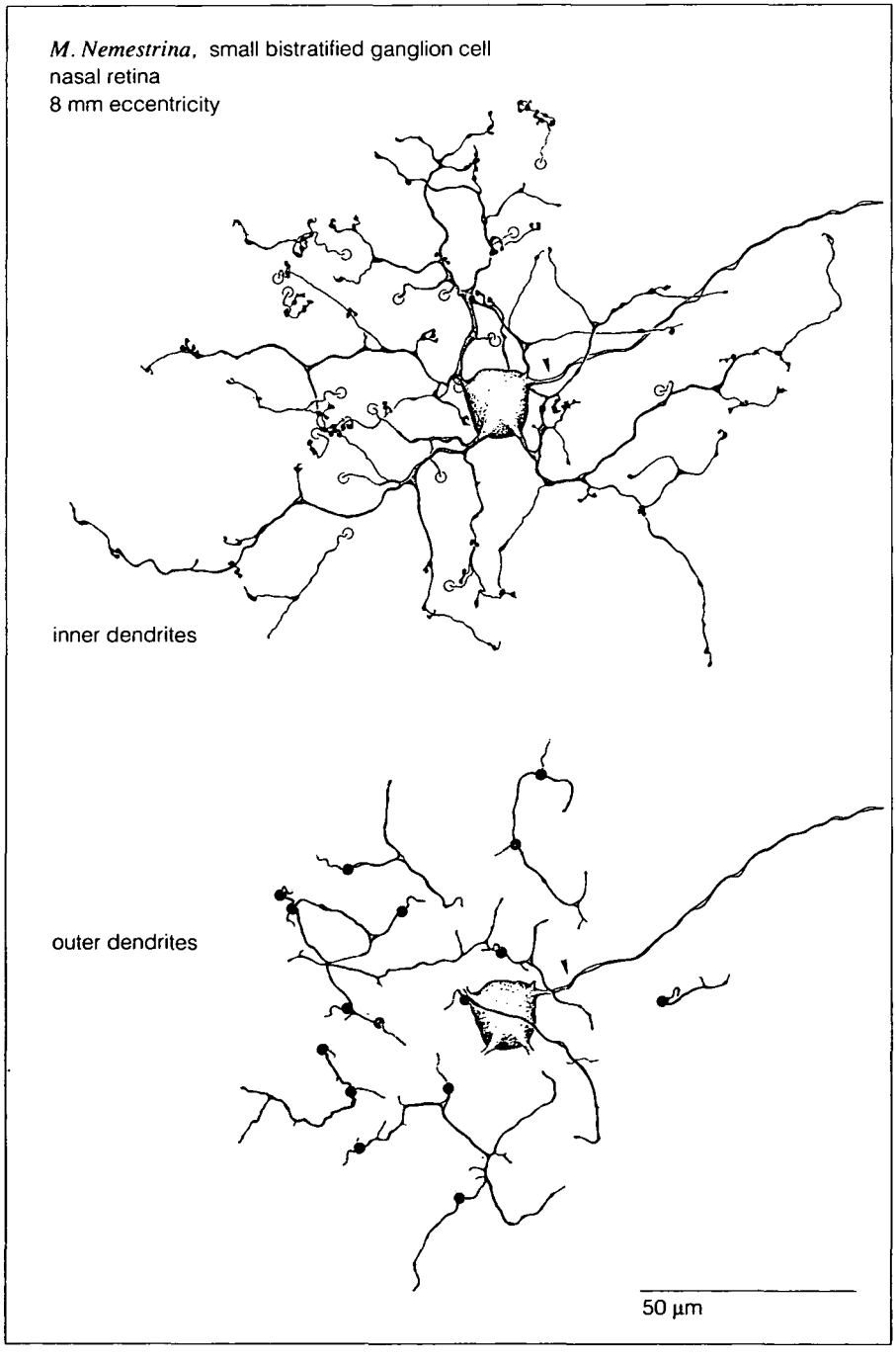

Fig. 4. Morphology of the small bistratified cell dendritic tree. Camera lucida tracing of the cell shown in Fig. 3A and 3B illustrates the main components of the bistratified dendritic morphology. The inner tier dendrites, shown at the top, give rise to distinct, spine-like branchlets that often bear large, lobulated heads. The outer tier dendrites (below), by contrast, are sparsely branching and relatively spine-free. The two dendritic tiers are connected by several thin, vertically running branches, illustrated as the hatched lines in the tracings. The connecting branches originate from all branch orders; their points of origin are indicated by the open (inner tier) and filled circles (outer tier). Arrowhead indicates axon near its point of origin from the soma.

tree (total magnification, 480× or 960×), and an outline of the cell body at higher magnification (1940×) was made. A measure of dendritic-field diameter was acquired for the intracellularly filled ganglion cells by tracing a convex polygon around the perimeter of the traced dendritic tree. The area of this polygon was then calculated by entering the outline into a computer *via* a graphics tablet. Dendritic-field diameter was expressed as the diameter of a circle with the same area as that of the polygon. Cell body size was similarly expressed in terms of an equivalent diameter.

The depth of stratification in the IPL of the small bistratified cell dendritic tree was evaluated in vertical serial sections in two cells from macaque retina. One cell was located in the upper retina at ~7 mm eccentricity, and the other cell was located in the temporal retina at 11 mm eccentricity. Camera lucida tracings were made of the cells before vertical sections were made. Both cells showed the characteristic morphology of the small bistratified cell type, including the characteristic tracer coupling to a single amacrine cell population. Tissue pieces containing the cells were embedded in plastic resin. Sections through the dendritic fields were cut at 10 μm with a glass knife and mounted on slides in serial order. A detailed camera luc-

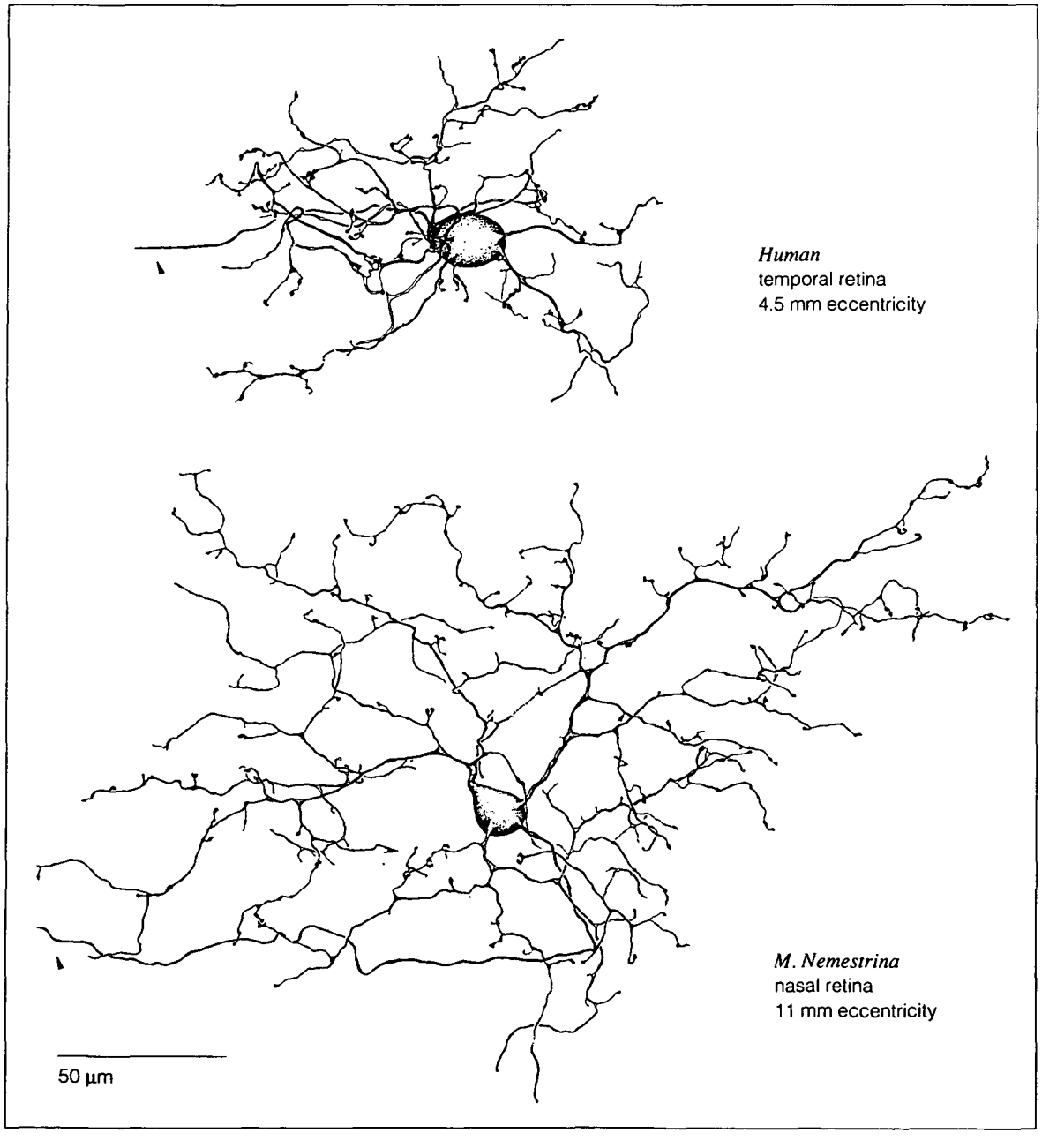

Fig. 5. Morphology of the small bistratified ganglion cell at two different retinal eccentricities. Upper cell from human temporal retina at 4.5 mm eccentricity. Lower cell from macaque nasal retina at 11 mm eccentricity. The characteristic morphology of both the inner (dark) and outer (light) dendritic tiers is preserved as overall dendritic-field size increases with retinal eccentricity. Axons are indicated by the arrowheads.

ida tracing of each section was made (total magnification 1940×) that included the outer and inner borders of the IPL and all HRP-labeled dendritic segments that were contained within that section. For both cells the stratification pattern appeared identical. The depth of stratification was quantified for one of the cells. The tracing of each section was placed on a graphics tablet and overlain with a grid of lines orthogonal to the retinal layers, and spaced 5 μm apart. The locations of the inner and outer borders of the IPL and the labeled dendrites that intersected each grid line were then entered into the computer. Measurements were made on every serial section that contained labeled dendrites. The relative depth of stratification was expressed as a percent of the total thickness of the IPL at each point of measurement and a histogram displaying all of the depth measurements was then compiled.

Results

Identification of the small-field bistratified cells

The sample of 81 macaque and 61 human intracellularly filled small bistratified cells forms the data base for this study. This sample was derived from a larger data base of intracellularly filled ganglion cells containing a diversity of morphological types (Dacey et al., 1991). In these experiments, no specific cellular marker was used to identify the small bistratified ganglion cell as distinct from all other ganglion cell types. However, as for the other common ganglion cells of the primate retina, the parasol and midget cells (Watanabe & Rodieck, 1989; Dacey & Brace, 1992; Dacey & Petersen, 1992), certain morphological features allowed this cell type to be unambiguously identified. First, the clearly bistratified nature of the dendritic tree allowed these cells to be distinguished categorically from all non-bistratified cells, and second, the relatively small size of the dendritic tree, in the general size range of the parasol ganglion cell, permitted these cells to be distinguished from other bistratified ganglion cell types with much larger dendritic fields. This distinction is shown in Fig. 1 in which dendritic-field size is plotted as a function of retinal eccentricity for the parasol, midget, and bistratified ganglion cells in the human retina data base (Dacey, 1993). The cells classed as small bistratified cells overlapped the parasol cells at all eccentricities sampled and did not overlap with the cluster of "large bistratified" ganglion cells. There were several other morphological features in addition to the small size that permitted the unequivocal identification of the small bistratified cells, including a characteristic pattern of tracer coupling to a mosaic of amacrine cells that was not observed for other types of bistratified ganglion cells. These properties will be considered further below.

Dendritic morphology

Although in the same dendritic-field size range as the parasol ganglion cell, the small bistratified ganglion cell displayed several distinctive morphological features that allowed it to be clearly distinguished in both macaque and human retina (Figs. 2A and 2B). The two dendritic tiers were clearly separated and morphologically distinct. The inner tier dendritic tree was larger in diameter and more densely branched than the outer tier (Figs. 3A and 3B); the inner branches also appeared thicker and gave rise to a sparse array of distinct spine-like branchlets (Figs. 3D and 3E). These branchlets were thin and long and ter-

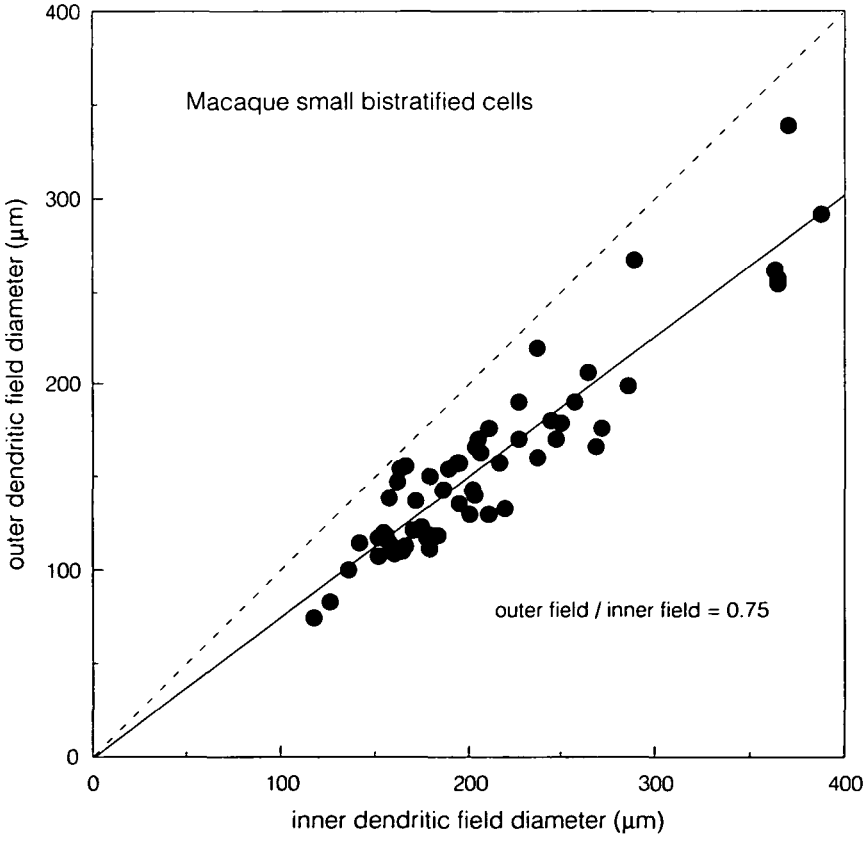

Fig. 6. Scatterplot of outer dendritic-field diameter as a function of inner dendritic-field diameter for the macaque small bistratified ganglion cells. In all cells, the outer tree is smaller than the inner tree and all points fall below the line of unity ratio (dotted line with slope of 1). The ratio of outer field to inner field diameter is ~0.75. Solid line through data points was fit by linear regression.

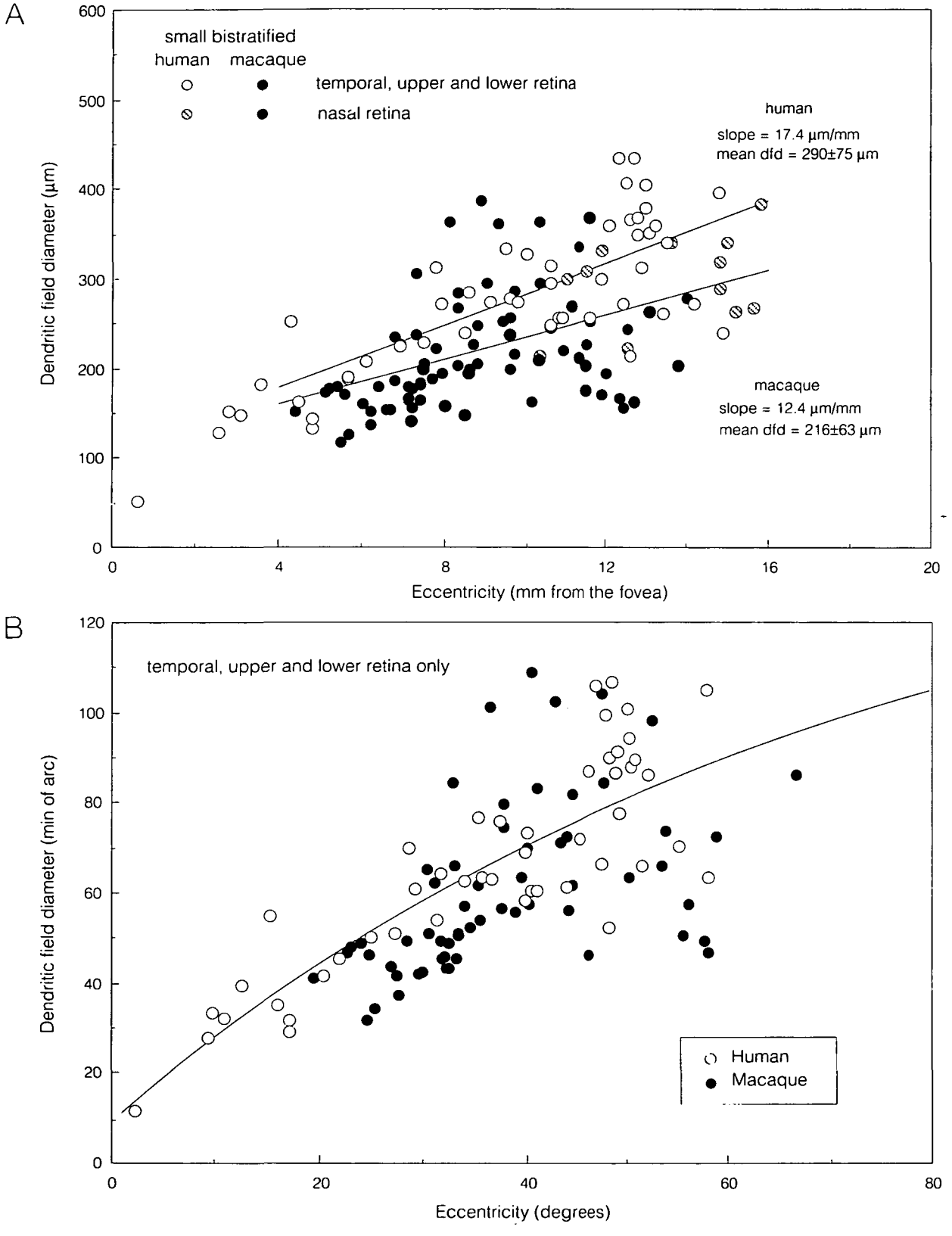

Fig. 7. Dendritic-field diameter for the small bistratified ganglion cells of the macaque and human retinas plotted as a function of retinal eccentricity. A: Human cells are on average 12–24% larger in dendritic-field diameter than their counterparts in the macaque. Regression lines fit to data from 4–16 mm eccentricity. In both species, cells in the nasal retina are somewhat smaller in diameter than in temporal, upper, or lower retina. B: Same cells plotted as in A but with dendritic-field diameter expressed in min of arc and eccentricity expressed in degrees of visual angle. The data have been corrected for differences in retinal magnification between human and macaque eyes in this plot (see Material and Methods). When the data is plotted in this way, the size difference between the two sets of data is not evident. The curve is a second-order polynomial fit to the human data ($R = 0.86$).

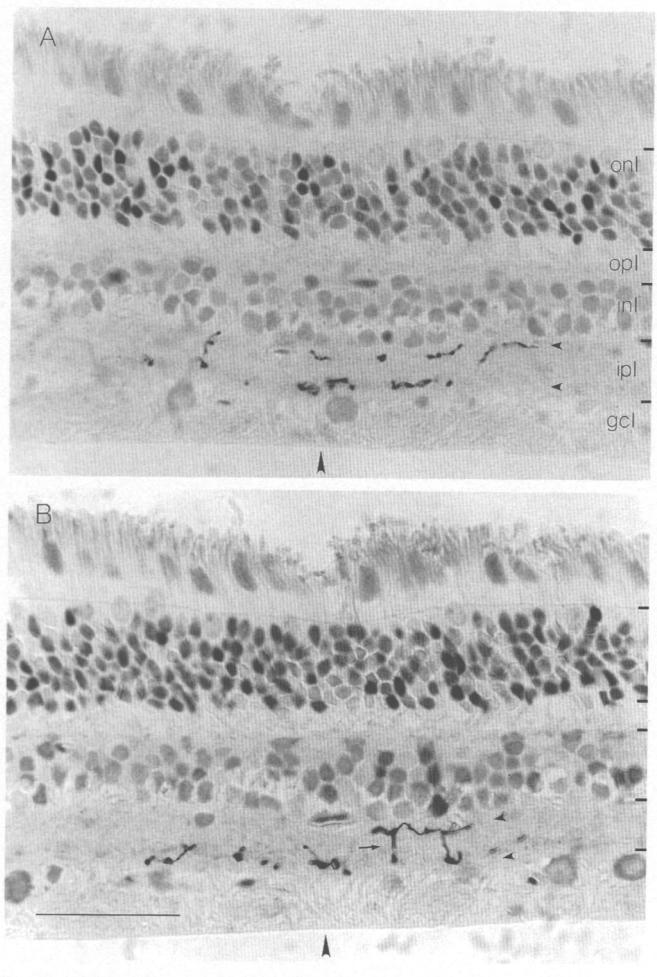

Fig. 8. Photomicrographs of dendritic stratification of the small bistratified ganglion cell in macaque. A,B: Two 8 μm-thick adjacent sections taken through the dendritic tree of a Neurobiotin filled cell. A: Segments of stained dendrites from both the inner and outer tier are present close to the inner and outer borders of the inner plexiform layer (small arrowheads). B: In the adjacent section, two vertical connecting branches between the two tiers are present (small arrow). Large arrowheads mark corresponding points in both sections. Scale bar = 50 μm.

minated in a relatively large, often lobulated head giving this part of the dendritic tree a characteristic appearance. The terminals of multiple branchlets occasionally converged to form small, loose aggregates. The spine-like branchlets could be easily distinguished from the more numerous simple spines present on the dendrites of parasol cells (Fig. 2A). The smaller, outer dendritic tier was composed of relatively thin branches that often showed a patchy distribution that did not uniformly fill the area of the dendritic field. These branches were relatively spine-free; any spines present tended to be small and simple compared to those of the inner dendritic tier. Several thin, vertically running twigs connected the two dendritic tiers and can best be illustrated in a camera lucida tracing of a small bistratified cell (Fig. 4). These connecting twigs arose from all branch orders including terminal dendrites. The inner and outer trees were therefore interconnected at multiple points across the dendritic field. The small bistratified cells increased in overall dendritic-field size with increasing distance from the fovea; however, the major features of dendritic morphology, the smaller, more sparsely branched outer tier and the larger, more densely branched inner tier, with its spine-like branchlets, were evident over the full range of dendritic-field diameters in the sample (Fig. 5).

Dendritic field and soma size

Fig. 6 plots the relative diameters of the inner and outer tier dendritic fields for the macaque small bistratified cells. For all cells the outer field was smaller than the inner field. The mean ratio of outer to inner field diameter was 0.75 and was well fit by a straight line over a fourfold change in overall dendritic-field size suggesting that the relative size difference is independent of retinal location, at least over the range sampled, and is a characteristic feature of this cell type.

Fig. 7 plots the relationship of largest, that is, the inner tier, dendritic-field diameter to retinal eccentricity for the small bistratified cells in both the human and macaque retina. From 4–16 mm eccentricity, the human cells were on average slightly larger in diameter than their macaque counterparts (Fig. 7A). Regression lines fit to the data (temporal, upper, lower fields only) from 4–16 mm eccentricity showed that the human cell cluster was shifted 12–24% upwards from the macaque. The

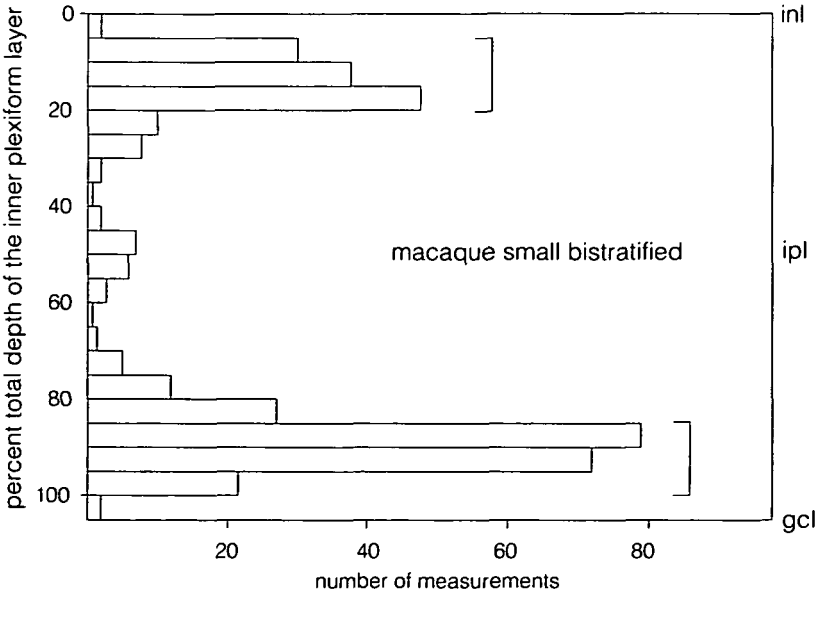

Fig. 9. Histogram of 376 measurements of dendritic depth for the cell shown in Fig. 8. About 50–60% of the dendritic tree (the inner tier) is stratified very close to the ganglion cell layer, from 85–100% depth (lower bracket) and ~30–40% of the tree (the outer tier) is stratified from 5–20% depth (upper bracket). The vertical connecting branches that extend through the depth of the inner plexiform layer therefore account for about 10% of the total dendritic tree.

mean size for the human cells (290 ± 75 μm) was 1.3 times that of the macaque (216 ± 63 μm). Cells located in the nasal quadrant tended to be smaller than those in the other quadrants for both species. A similar observation has been made for the parasol and midget ganglion cells (Watanabe & Rodieck, 1989; Dacey & Petersen, 1992).

When the difference in retinal magnification between macaque and human eyes is taken into account and the dendritic-field size in minutes of arc is plotted as a function of eccentricity in degrees of visual angle, the macaque and human cell clusters become more highly overlapped at all the eccentricities sampled (Fig. 7B). A second-order polynomial curve fit to the human data ($R = 0.86$) from the temporal, upper, and lower fields suggests that the small bistratified cells range in size from about 10 min arc in the central retina to about 1.3 deg in the far retinal periphery.

The soma diameters of human small bistratified cells (18.9 ± 2.4 μm, $n = 61$) were also larger than for their counterparts in the macaque retina (15.9 ± 1.05 μm, $n = 81$). This follows the finding that the midget and parasol ganglion cell types have larger soma diameters in the human than in macaque (Watanabe & Rodieck, 1989). The scaling does not appear to be uniform across different ganglion cell types however. The human midget cells show a greater increase in soma size over the macaque than the other major ganglion cell types. A consequence is that in the macaque retina the small bistratified cells are similar in soma size to the parasol ganglion cells, but in the human retina they are closer in soma size to the larger bodied midget ganglion cells. These soma size relationships between the parasol, midget, and small bistratified cell types are summarized in Table 1.

Depth of dendritic stratification

In retinal wholemounts, the small bistratified cells appeared to be narrowly stratified near the inner and outer borders of the IPL in both the human and macaque. The bistratification was quantified for a single cell by measuring the depth of the dendritic branches in serial radial sections through the dendritic tree (Figs. 8A and 8B). A histogram of this data (Fig. 9) shows that most of the dendritic tree was located in two narrow strata, each occupying about 15% depth of the IPL, near its inner and outer borders. About 50–60% of the dendrites were stratified between 85–100% depth and about 35% of the dendrites were between 5–20% depth. The remaining 10% of the dendrites were spread out thinly between the two strata, consistent with the interpretation that they represented minor vertical connections between the two major strata.

Table 1. *Soma size ranges for midget, small bistratified, and parasol ganglion cells*

Cell type	Macaque	Human	Human-macaque ratio
Midget	12.1 ± 1.9[a,b] ($n = 148$)	17.9 ± 2.5[c] ($n = 334$)	~1.5
Parasol	17.4 ± 2.7[b] ($n = 500$)	23.3 ± 3 ($n = 265$)	~1.35
Small bistratified	15.9 ± 1.1 ($n = 81$)	18.9 ± 2.4 ($n = 61$)	~1.2

[a]All data given as mean ± standard deviation.
[b]Soma size data from Watanabe and Rodieck (1989).
[c]Mean of inner (presumed ON-center) and outer (presumed OFF-center) branching types. Mean ± S.D. for inner cells: 18.6 ± 2.3 μm, $n = 156$; outer cells: 17.4 ± 2.3 μm, $n = 178$ (Dacey, 1993).

Homotypic and heterotypic coupling

Intracellular injections of Neurobiotin in the macaque retina revealed intense tracer coupling between the small bistratified cells and an overlying mosaic of amacrine cells (Figs. 10A and 10B). Several aspects of the amacrine staining suggested strongly that only a single amacrine cell type was coupled to the small

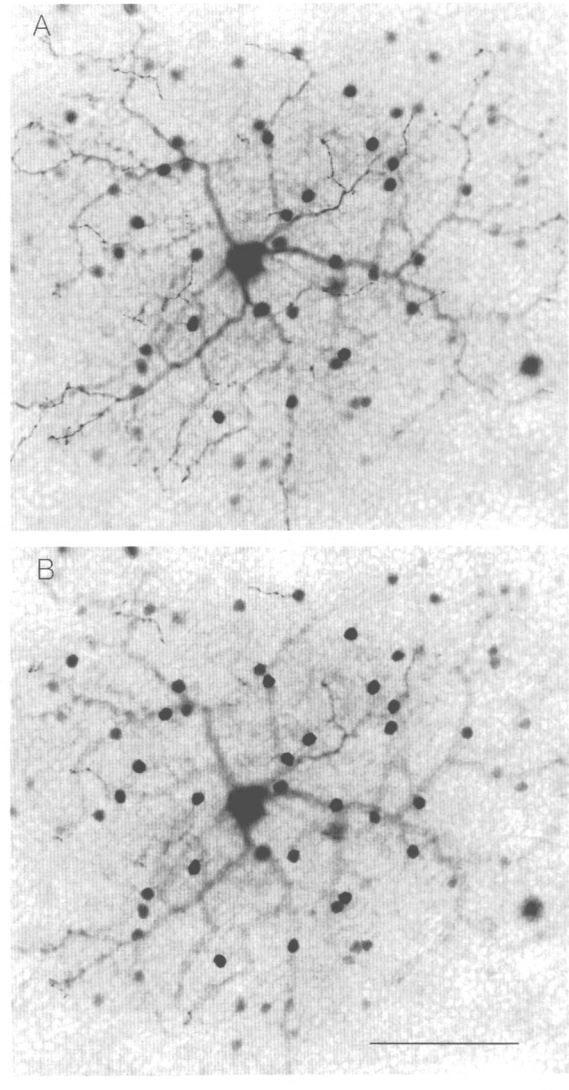

Fig. 10. Photomicrograph of tracer coupling between the small bistratified ganglion cell and an amacrine cell population in the macaque retinal periphery. A: Plane of focus is at the outer tier of dendrites; many small darkly stained amacrine cell bodies are slightly out of the plane of focus. B: Plane of focus shifted to the amacrine cell layer; a regular array of very small cell bodies (~8 μm in diameter) are intensely stained within the bounds of the dendritic field. The amacrine cell staining gradually fades with increasing distance from the injected ganglion cell. Scale bar = 100 μm.

bistratified cell. First, coupled cells were arranged in a regular mosaic. The mean distance between nearest neighbors in the mosaic was 23 ± 4.75 μm giving a regularity index (mean/S.D.) of 4.8, which is similar to that found for other well-defined retinal cell mosaics (Wässle & Riemann, 1978), and in particular matches the degree of regularity found for another identified small-field amacrine cell type, the AII amacrine (Vaney, 1985). Second, the small, round cell bodies were all similar in appearance and in diameter (mean = 8.1 μm, S.D. = ±0.4, n = 137). The dendritic morphology, as far as it could be observed, also appeared uniform. The overall staining of the dendritic tree was faint; however, in some of the more intensely stained examples it was possible to discern some aspects of the dendritic structure. The amacrine cells appeared to be bistratified in the IPL at the same depths as the stained ganglion cell. The dendritic tree was compact, roughly about 100 μm in diameter in the retinal periphery and composed of very densely branched, fine varicose processes. Spatial density in the periphery was ~1700 amacrine cells/mm^2. About 70% of the small bistratified cells (55 of 81 cells) showed this distinctive type of amacrine cell cou-

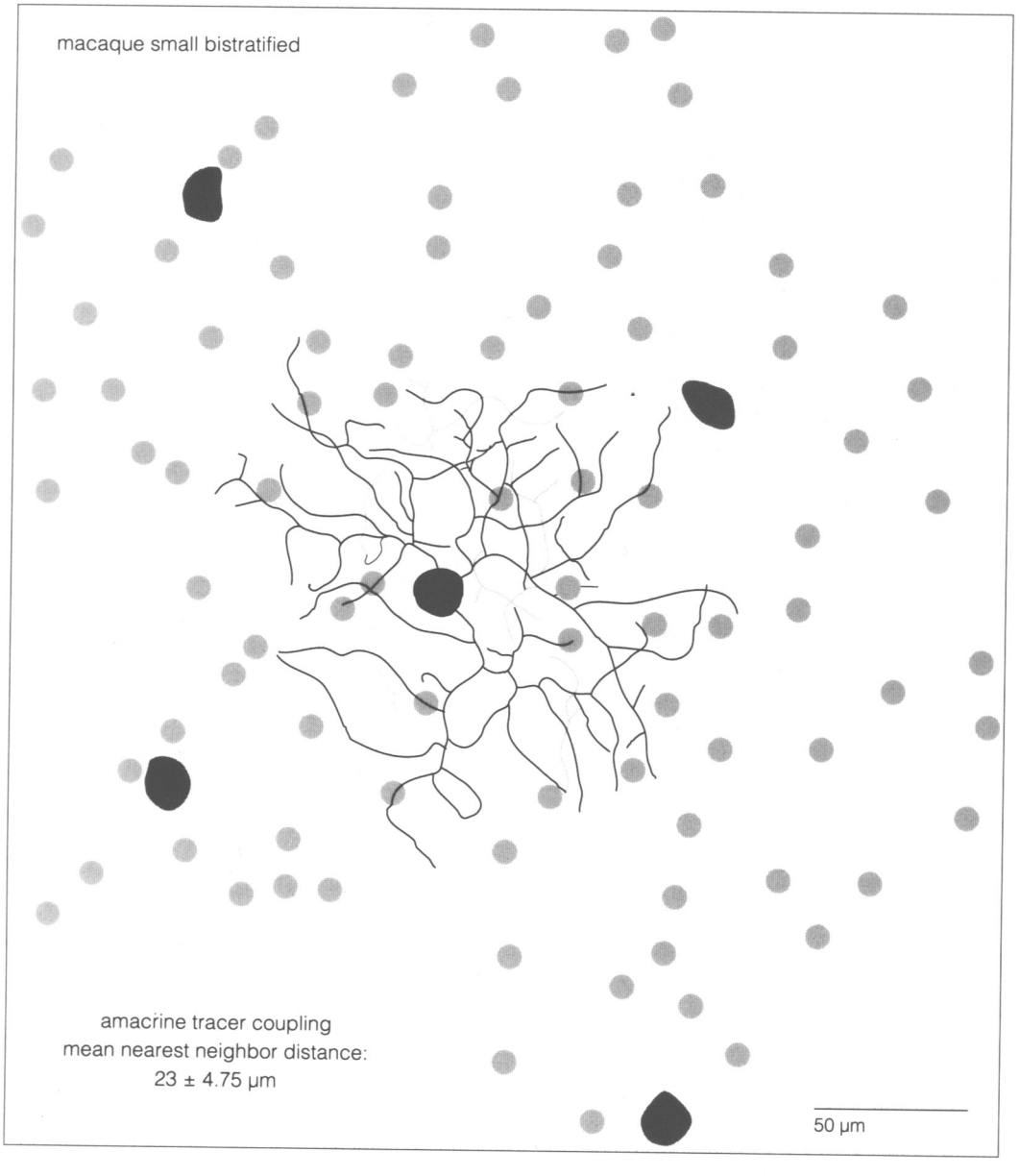

Fig. 11. Mosaic organization of tracer coupling to the small bistratified ganglion cell type in macaque. Simple tracing of the dendritic branching pattern of a small bistratified cell (solid: inner tier dendrites; shaded: outer tier dendrites) and all of the cells in the amacrine cell layer (small, lightly shaded circles) and ganglion cell layer (larger, darkly shaded profiles) that showed tracer coupling to this cell. Mean nearest-neighbor distance for this patch of amacrine cells is 23 ± 4.7 μm. The ratio of mean distance to standard deviation is 4.8, suggestive of a non-randomly arranged mosaic (Wässle & Riemann, 1978). The uniform soma size and the regular spatial arrangement of these amacrine cells suggest that only a single amacrine cell type is tracer-coupled to the small bistratified cell. The size and location of the larger cells in the ganglion cell layer suggest that they are neighboring ganglion cells of the same type.

pling and it was thus a relatively reliable marker for the small bistratified ganglion cell type.

In addition to the heterotypic amacrine cell coupling, several cells (11 of 55, 20%) also showed some evidence of homotypic coupling, that is, coupling to neighboring ganglion cells of the same type (Figs. 11 and 12A). This occurred in the cells with the most intensely stained amacrine mosaic and appeared as a relatively light staining of a ring of large cell bodies located in the ganglion cell layer and surrounding the perimeter of the dendritic tree of the injected ganglion cell. Little of the dendritic tree of these coupled cells was revealed so that they cannot be identified with certainty. However, the ganglion cells were spaced at a regular distance from each other suggestive of a mosaic organization, and in a few instances lightly stained dendrites did reveal bistratification. The mean ± S.D. nearest-neighbor distance was 132 ± 26 μm ($n = 49$) giving a regularity index of 5.0 which is in the range found for other ganglion cell mosaics (Wässle & Riemann, 1978). Previous studies have revealed a similar pattern of homotypic tracer coupling for the alpha ganglion cells of the cat, the ON-OFF direction-selective cells of the rabbit (Vaney, 1991), and the parasol ganglion cells of the macaque (Dacey & Brace, 1992).

Fig. 12B plots the relationship of nearest-neighbor distances to the diameters of the inner and outer dendritic fields for the small bistratified cells that showed ganglion cell tracer coupling. The mean ratio of near-neighbor distance to inner-field diameter was 0.71 and that for the outer field was 0.97. Assuming hexagonal packing, these ratios give a coverage for the inner and outer tier dendritic fields of ~1.8 and 1.0, respectively. How this kind of intercell spacing would appear relative to the inner and outer dendritic fields is illustrated in the inset in Fig. 12B.

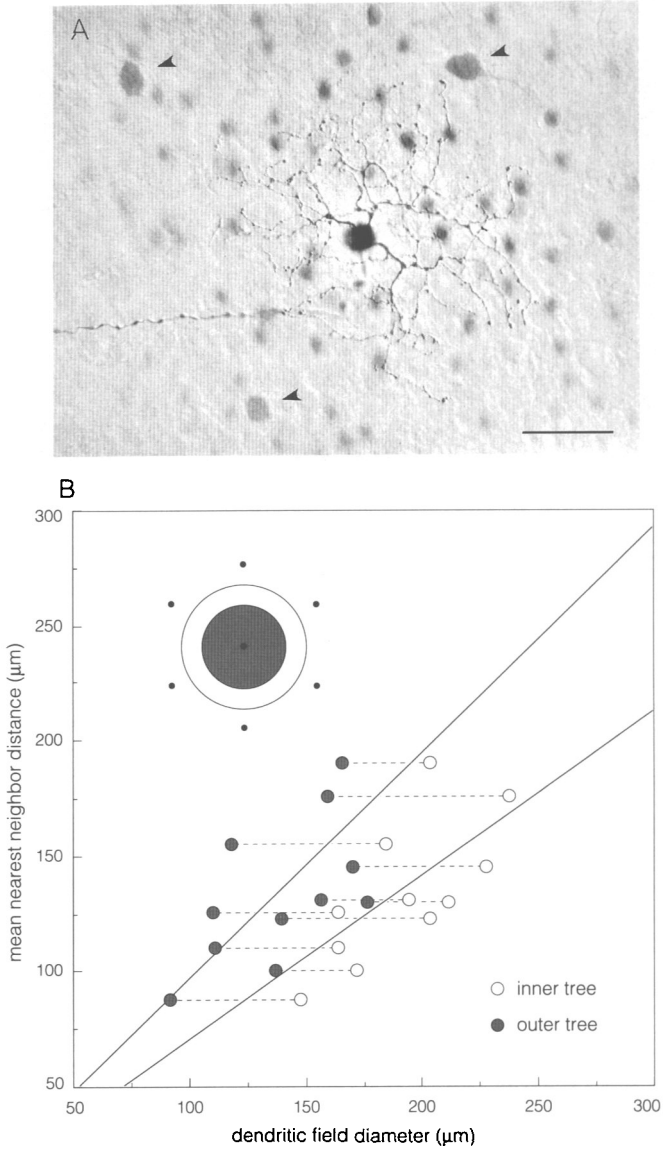

Fig. 12. Tracer-coupled ganglion cells show a regular arrangement and suggest a dendritic coverage for the inner and outer dendritic trees. A: Photomicrograph of a small bistratified cell in macaque that showed tracer coupling to ganglion cells around the perimeter of the injected cell's dendritic tree (arrowheads). Plane of focus on inner tier dendrites. Scale bar = 50 μm. B: Plot of mean nearest-neighbor distance as a function of inner and outer dendritic field diameter for 11 small bistratified ganglion cells that showed ganglion cell tracer coupling. Regression lines are fit through data for inner and outer fields. Inner and outer field diameters for each cell are linked by the dotted lines. Ratio of near-neighbor distance to inner and outer field diameter is 0.71 and 0.95, respectively. Inset shows the spatial distribution of the neighboring cell bodies (solid dots) relative to the inner (larger open circle) and outer tree (smaller shaded circle) given by the ratios shown in the plot and arranged hexagonally, corresponding to an approximate coverage factor of 1.8 and 1.

Discussion

Previous observations

Though not explicitly identified, it seems likely that some hint of the small bistratified ganglion cell type can be found in the classical Golgi studies of the primate retina. Some of the cells that Polyak (1941) denoted as "shrub" cells and Boycott and Dowling (1969) termed "diffuse" cells may include the small bistratified cell, as it is these cells that display dendritic fields in the right size range. The shrub and diffuse cells may also possess a bistratified morphology, as originally noted by Rodieck (1973; his Table XV-3), who suspected that Ramon y Cajal might have categorized them as bistratified. Figs. 71n and 69n (reproduced by Rodieck et al., 1985, as their Fig. 2) of Polyak (1941) and Fig. 84 of Boycott and Dowling (1969) appear bistratified to some degree. Polyak and Boycott and Dowling observed Golgi impregnated cells in vertical sections through the retina. A frequently noted difficulty in identifying multistratified cells in vertical sections is that slight deviations from the vertical plane will make dendrites appear to branch through a greater depth of the IPL than is actually the case (e.g. Amthor et al., 1984; Boycott & Dowling, 1969). Boycott and Dowling noted that the cell pictured in their Fig. 84 (and referred to above) was observed directly from the side in a perfect vertical section, and it is this cell that appears to show a bistratified morphology most clearly; indeed with hindsight it further appears that the major strata lie close to the inner and outer border of the IPL, as found for the small bistratified cells of the present study.

More recently, the use of intracellular injections of horseradish peroxidase in an *in vitro* preparation of the macaque retina revealed the small bistratified cells clearly for the first time (Rodieck et al., 1987). One reason that the bistratified cells were recognized was that in retinal wholemounts the two distinct den-

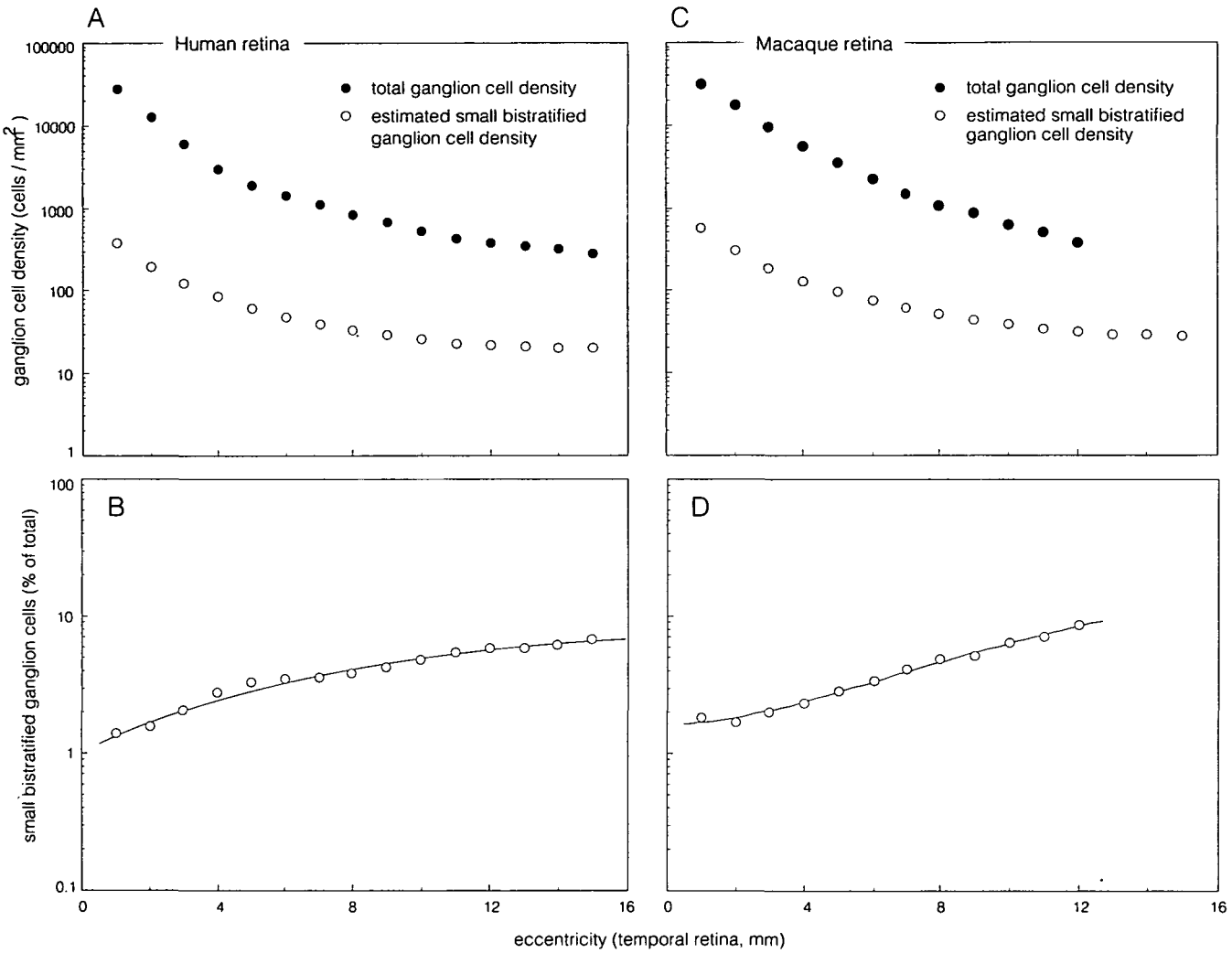

Fig. 13. Estimate of spatial density as a function of eccentricity for the small bistratified ganglion cells in macaque and human retina. A: Plot of total ganglion cell density (taken from Curcio & Allen, 1990; mean of temporal, superior, and inferior meridian values) and estimated density of the small bistratified ganglion cells as a function of retinal eccentricity. Small bistratified cell density was calculated by dividing dendritic field coverage (Fig. 12) by dendritic field area (Fig. 7) assuming constant overlap across the retina and hexagonal cell packing. B: The percentage of small bistratified cells in the human retina plotted as a function of retinal eccentricity. The proportion of small bistratified cells increases from ~1% of the total in the central retina to ~6% in the far periphery. C: As in (A) but for macaque retina (total ganglion cell density from Perry & Cowey, 1985; mean of temporal, upper, and lower meridian values). D: In macaque the percentage of small bistratified cells increases from ~1.5% centrally to ~8.5% peripherally. The relatively high spatial density of the small bistratified ganglion cell type suggests that it is the most numerous ganglion cell type beyond the ON- and OFF-center midget and parasol ganglion cell types.

dritic strata can be easily appreciated by focusing through the thickness of the retina. Subsequently, these cells were observed by intracellular HRP filling of ganglion cells that had been retrogradely labeled from a tracer injection made into the parvocellular layers of the dorsal lateral geniculate nucleus (Rodieck, 1991). In the present results, a large data base has permitted a more detailed description of this cell type in both the macaque and human retina using a similar intracellular injection technique. Fig. 14 shows a comparison of the morphology of the small bistratified ganglion cell with the two other common ganglion cell types of the primate retina, the midget and parasol cells. Aside from differences in dendritic-field size, all three cell types can be easily distinguished by the characteristic branching patterns of their dendritic trees.

Estimate of the spatial density of the small bistratified cell

By combining the data on dendritic-field size (Fig. 7) and the measurements of intercell spacing from the cells that showed homotypic coupling (Fig. 12), it was possible to make an estimate of the spatial density of the small bistratified cells in both the macaque and human retina. This estimate assumes a constant coverage across the retina and must therefore be viewed as provisional; if it is shown that coverage changes significantly in the central retina, then the calculated cell densities would not be accurate. In human, the estimated small bistratified cell density ranges from ~400 cells/mm^2 in central retina, dropping to ~20 cells/mm^2 in the retinal periphery (Fig. 13A). In relation to total ganglion cell density however, the small bistrat-

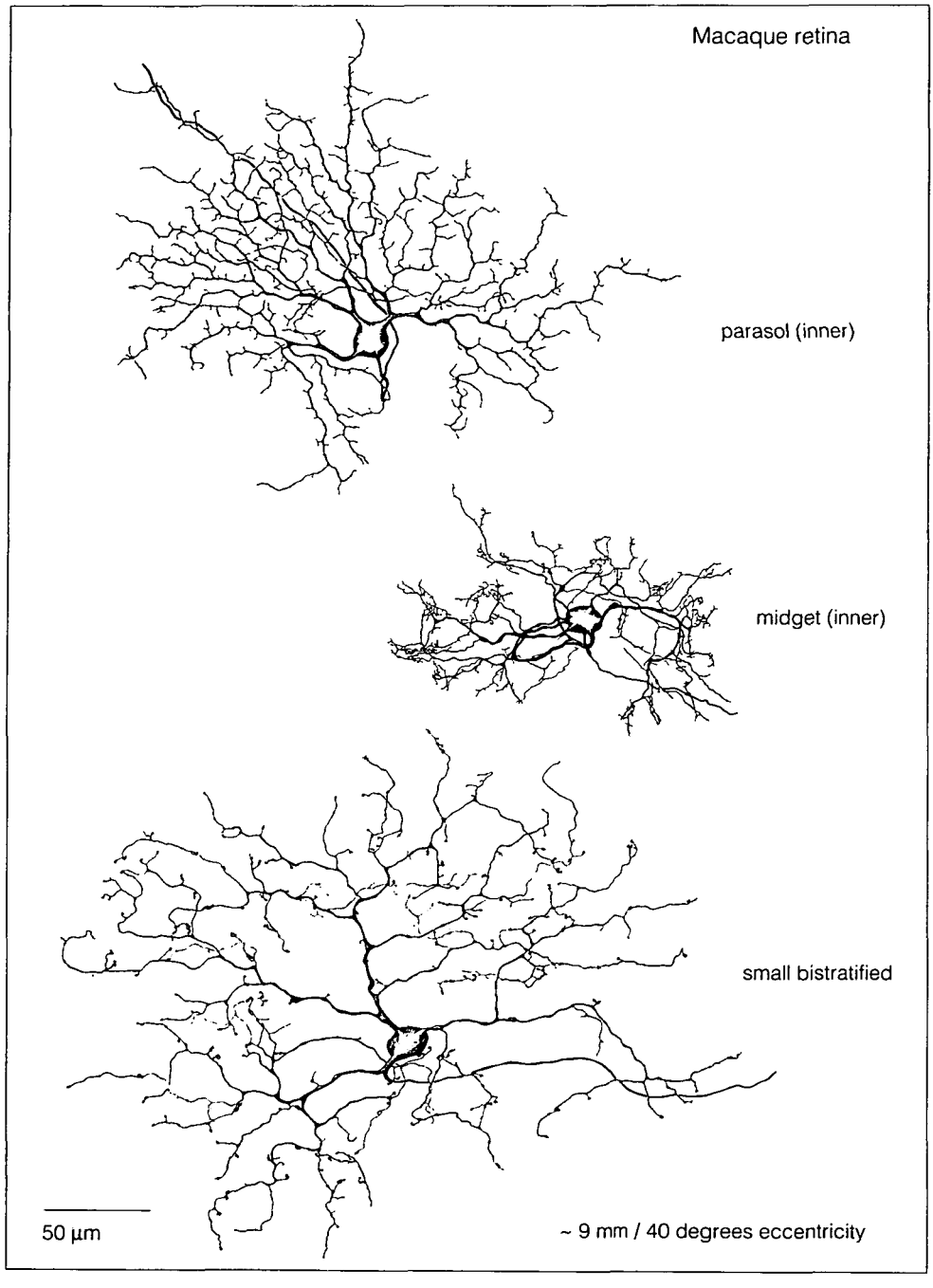

Fig. 14. A comparison of the morphology of the parasol, midget, and small bistratified ganglion cell types in the macaque and human retina. Examples of each cell type are shown at about the same eccentricity in degrees of visual angle for both species. A distinctive dendritic morphology is apparent for each cell type. Parasol cells are narrowly stratified, spiny, and relatively densely branching and distribute their branches rather uniformly within the dendritic field. Midget cells have very fine dendritic branches that are distributed nonuniformly in the dendritic field: terminal dendrites arborize into several clusters separated by clear gaps. Small bistratified cells are more sparsely branched than the parasol cells and show distinctive spine-like branchlets. In both species, the basic morphology of the cell types is recognizable; note however that the midget and small bistratified cells show the same dendritic-field diameter in human and macaque but that the human parasol cell is about 30% larger in diameter than its counterpart in the macaque; thus the small bistratified cell is smaller or equivalent in size to the parasol in the human retina but is slightly larger than the parasol cell in the macaque retina.

ified cells increase from ~1% of total cell density centrally to ~6% in the retinal periphery (Fig. 13B). In macaque, the smaller dendritic-field size for the small bistratified cell gives a somewhat higher range of densities from ~500 cells/mm^2 in the central retina to ~30 cells/mm^2 in the retinal periphery (Fig. 13C). As for the human, the percentage of macaque small bistratified cells increases from ~1.5% centrally to ~8.5% peripherally (Fig. 13D). The relatively high spatial density of

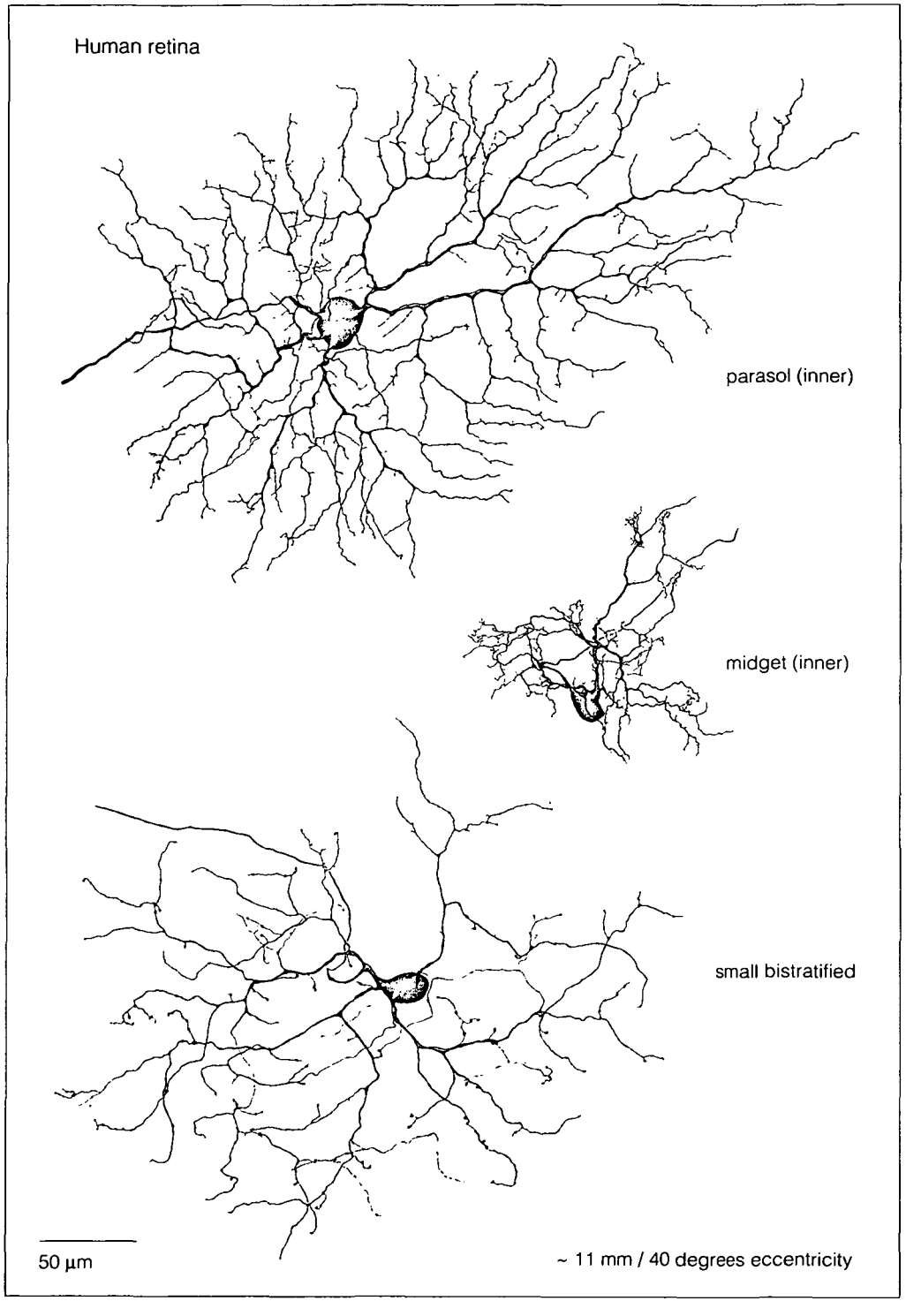

Figure 14 continued.

the small bistratified ganglion cell type suggests that it is the most numerous ganglion cell type beyond the ON- and OFF-center midget and parasol ganglion cell types.

The accuracy of the finding that the proportion of small bistratified cells changes as a function of eccentricity is critically dependent on accurate cell counts for the total ganglion cell population, especially in central retina where density changes rapidly. For example, a recent study found peak ganglion cell density to be 60,000 cells/mm^2 (Wässle et al., 1990) almost twice that found in a previous study of macaque (Perry & Cowey, 1985). This higher foveal value for total ganglion cell density would give a percentage of less than 1 in central retina for the small bistratified ganglion cell.

That the small bistratified cells become proportionately less

numerous in the central retina is significant in view of recent results concerning the relative densities of the other major primate ganglion cell types. Although there is some evidence that the percentage of midget and parasol ganglion cells remains proportional across the retina at roughly 80% and 10% (Livingstone & Hubel, 1988; Perry et al., 1984), recent studies of the midget ganglion cell mosaic in human retina suggest that the percentage of midget ganglion cells increases from ~45% of the total in the retinal periphery to about 95% centrally (Dacey, 1993). This finding is consistent with the suggestion that the ratio of midget to parasol cells changes with eccentricity such that parasol cells decrease in relative numbers in the central retina (Drasdo et al., 1991; Schein & de Monasterio, 1987; Dacey & Petersen, 1992). The proportionate decrease in small bistratified cell density towards the fovea suggests that the midget ganglion cells show a steeper density gradient relative to this cell type as well.

Does the small bistratified cell co-stratify with either the midget or parasol ganglion cell type?

The narrow stratification of the small bistratified ganglion cell close to the inner and outer borders of the IPL means that it would be very unlikely to overlap the strata occupied by the parasol ganglion cells. The inner, presumed ON-center, and outer, presumed OFF-center, parasol types are narrowly stratified near the center of the IPL at ~35% and 65% depth in both the macaque (Watanabe & Rodieck, 1989) and human retina (Petersen et al., 1991). The situation is less clear for the midget ganglion cells. In both macaque and human retina, the inner and outer midget ganglion cell types extend closer to the outer and inner borders of the IPL than do the parasol ganglion cells (Watanabe & Rodieck, 1989; Dacey, 1993). The outer dendritic tier of the small bistratified ganglion cell may thus co-stratify with at least a part of the midget cell dendritic tree. It is less likely that the inner tier dendrites of the small bistratified cell overlap with the inner midget cell dendritic tree. In human retina, analysis of vertical sections suggested that inner midget cell dendrites did not extend into the inner 10% of the IPL. This sublayer is occupied principally by the rod bipolar, blue-cone bipolar, and a single diffuse cone bipolar type, but not by the midget bipolar cell axon terminals (Boycott & Wässle, 1991; Grünert & Martin, 1991).

Tracer coupling to amacrine cells

The tracer-coupled amacrine mosaic appears to be composed of cells with relatively small, densely branching dendritic trees that are also bistratified at the same depth as the ganglion cell type. Has this amacrine cell type been observed previously? One identified amacrine with a small, bistratified dendritic field is the AII amacrine cell, the principal amacrine cell type in the rod signal pathway (e.g. Strettoi et al., 1992). This cell type makes sign-conserving synapses with ganglion cells in the ON sublayer of the IPL and sign-inverting chemical synapses in the outer, OFF sublayer. The tracer-coupled amacrine observed in the present study was clearly not the AII amacrine cell however, as its dendrites bore no resemblance to the arboreal and lobular dendrites of the AII amacrine. The very fine, varicose and densely branched processes of the tracer-coupled amacrine suggests instead a correspondence to a general class of amacrines observed in Golgi preparations of the macaque retina, the 'knotty' amacrine cells, of which bistratified examples have been found (Mariani, 1990; Polyak, 1941).

Significance of small bistratified cells for color processing

Some predictions can be made about the physiology of the small bistratified cell based on the anatomy described here and on its projection to the parvocellular lateral geniculate reported previously (Rodieck, 1991). Its projection is consistent with color opponency, although some non-opponent cells have been recorded in the parvocellular layers (Wiesel & Hubel, 1966; Dreher et al., 1976). The bistratification is suggestive of an ON-OFF response to light; a few ON-OFF cells have been recorded in the macaque retina but they do not show color opponency and probably do not project to the parvocellular layers (de Monasterio, 1978). Rodieck (1991) hypothesized that the bistratified cells might carry both red-green and blue-yellow opponent signals and provide a non-midget ganglion cell color-coding pathway to the parvocellular layers. The present results cannot rule out this possibility; however, some features of the morphology of the small bistratified ganglion cell type suggest an exclusive correspondence to the blue-ON receptive-field unit. Blue-ON cells have larger receptive fields than the red-green opponent cells, consistent with the larger dendritic-field size of the small bistratified cell relative to the midget ganglion cells (see Zrenner et al., 1990, for a recent review). The estimated density of the small bistratified cells (2–8%) is also consistent with the sampling rate (~5–10%) of the blue-ON cells and the depth of dendritic stratification provides indirect evidence that the small bistratified cell receives direct synaptic input from a blue-cone signal pathway. Blue-cone bipolar cells terminate close to the inner border of the IPL, where they make synaptic contact with ganglion cell dendrites (Marshak et al., 1990; Kouyama & Marshak, 1992). The blue-cone bipolar stratum matches closely that of the inner tier of dendrites of the small bistratified cell (Figs. 8 and 9; compare with Fig. 4 of Kouyama and Marshak). By contrast the axonal terminals of the invaginating midget cone bipolar cells, that are presumably conveying red- and green-cone signals, terminate more sclerad than the blue-cone bipolar axon (Boycott & Wässle, 1991).

If the small bistratified cells corresponded to the blue-ON cells, what would be the significance of the bistratified dendritic tree? As noted above, an ON-OFF response to light might be expected, but the blue-ON yellow-OFF cells of the macaque retina have not been described as ON-OFF. Most blue-ON cells show coextensive receptive-field organization, that is, the center and "surround" are about the same size (e.g. Wiesel & Hubel, 1966; Derrington et al., 1984); indeed this type of receptive field has been considered by some to be an identifying property of the blue-ON cells (e.g. Zrenner & Gouras, 1981; Lennie & D'Zmura, 1988). It is possible that combined red and green cone input to the "surround" of the blue-ON cell may actually be derived from a diffuse cone bipolar input to the outer dendrites (Boycott & Wässle, 1991). If this were the case, the input to the smaller and more sparsely branched outer dendritic field might give rise to a relatively weak OFF response that could be mistaken for a kind of "surround" effect. Something like this has been found for the ON-OFF directionally selective ganglion cells of the rabbit retina: a cell with a larger and more extensive inner tree is associated with a stronger ON response (Amthor et al., 1984).

Other evidence regarding the morphology of the blue-ON cells can be found in the first attempt to link morphology and physiology in the primate retina using intracellular dye injection (de Monasterio, 1979). de Monasterio labeled three blue-ON cells and found that they stratified in the outer half of the IPL and had larger cell bodies (~15-24 μm) and larger dendritic-field diameters (~50 μm in central retina) than the red-green cells. His suggestion that the blue-ON cells correspond to the parasol ganglion cells seems unlikely, given our current knowledge of the parasol cell projection to the magnocellular lateral geniculate nucleus. The relatively large dendritic field and soma size for the blue-ON cell is, however, in line with the morphology of the small bistratified ganglion cell. On the other hand, the reported stratification of a blue-ON-center cell only in the outer part of the IPL does not fit with the hypothesis that these cells correspond to the small bistratified cells; as noted by De Monasterio this result was at the time, and still remains, an exception to the rule that ON-center ganglion cells have dendrites in the inner IPL.

Acknowledgments

I am especially grateful to Kim Allen and the staff of the Lions Eye Bank for the timely retrieval of donor eyes for this research. Kate Mulligan and Helen Sherk offered helpful comments on all aspects of this study. Dan Possin and Sarah Brace provided technical assistance, and the photographers of the Department of Ophthalmology, University of Washington provided excellent service. This work was supported by USPHS Grants EY 06678 (D.M.D.), EY01730 (Vision Research Core), and RR00166 to the Regional Primate Center at the University of Washington.

References

AMTHOR, F.R., OYSTER, C.W. & TAKAHASHI, E.S. (1984). Morphology of ON-OFF direction-selective ganglion cells in the rabbit retina. *Brain Research* **298**, 187-190.

BOYCOTT, B.B. & DOWLING, J.E. (1969). Organization of the primate retina: Light microscopy. *Philosophical Transactions of the Royal Society B* (London) **255**, 109-184.

BOYCOTT, B.B. & WÄSSLE, H. (1991). Morphological classification of bipolar cells of the primate retina. *European Journal of Neuroscience* **3**, 1069-1088.

CREUTZFELDT, O.D., LEE, B.B. & ELEPFANDT, A. (1979). A quantitative study of chromatic organization and receptive fields of cells in the lateral geniculate body of the rhesus monkey. *Experimental Brain Research* **35**, 527-545.

CURCIO, C.A. & ALLEN, K.A. (1990). Topography of ganglion cells in human retina. *Journal of Comparative Neurology* **300**, 5-25.

DACEY, D.M. (1989). Axon-bearing amacrine cells of the macaque monkey retina. *Journal of Comparative Neurology* **284**, 275-293.

DACEY, D.M. (1993). The mosaic of midget ganglion cells in the human retina. *Journal of Neuroscience* (in press).

DACEY, D.M. & BRACE, S. (1992). A coupled network for parasol but not midget ganglion cells of the primate retina. *Visual Neuroscience* **9**, 279-290.

DACEY, D.M. & PETERSEN, M.R. (1992). Dendritic-field size and morphology of midget and parasol ganglion cells of the human retina. *Proceedings of the National Academy of Sciences* **89**, 9666-9670.

DACEY, D.M., PETERSEN, M. & ALLEN, K. (1991). Beyond the midget and parasol ganglion cells of the human retina. *Investigative Ophthalmology and Visual Science* (Suppl.) **32**, 1130.

DE MONASTERIO, F.M. & GOURAS, P. (1975). Functional properties of ganglion cells of the rhesus monkey retina. *Journal of Physiology* (London) **251**, 167-195.

DE MONASTERIO, F.M. (1978). Properties of ganglion cells with atypical receptive-field organization in retina of macaques. *Journal of Neurophysiology* **41**, 1435-1449.

DE MONASTERIO, F.M. (1979). Asymmetry of ON and OFF pathways of blue-sensitive cones of the retina of macaques. *Brain Research* **166**, 39-48.

DERRINGTON, A.M., KRAUSKOPF, J. & LENNIE, P. (1984). Chromatic mechanisms in lateral geniculate nucleus of macaque. *Journal of Physiology* **357**, 241-265.

DE VALOIS, R.L., ABRAMOV, I. & JACOBS, G.H. (1967). Single-cell analysis of wavelength discrimination at the lateral geniculate nucleus in the macaque. *Journal of Neurophysiology* **30**, 415-433.

DRASDO, N. & FOWLER, C.W. (1974). Nonlinear projection of the retinal image in a wide-angle schematic eye. *British Journal of Ophthalmology* **58**, 709-714.

DRASDO, N., THOMPSON, C.M. & DEELEY, R.J. (1991). Psychophysical evidence of two gradients of neural sampling in peripheral vision. In *From Pigments to Perception*, ed. VALBERG A. & LEE, B.B., pp. 189-192. New York: Plenum Press.

DREHER, B., FUKUDA, Y. & RODIECK, R.W. (1976). Identification, classification, and anatomical segregation of cells with X-like and Y-like properties in the lateral geniculate nucleus of Old World primates. *Journal of Physiology* **258**, 433-453.

GRÜNERT, U. & MARTIN, P.R. (1991). Rod bipolar cells in the macaque monkey retina: Immunoreactivity and connectivity. *Journal of Neuroscience* **11**, 2742-2758.

HEIMER, G.V. & TAYLOR, C.E.D. (1974). Improved mountant for immunofluorescent preparations. *Journal of Clinical Pathology* **27**, 254-256.

KOUYAMA, N. & MARSHAK, D.W. (1992). Bipolar cells specific for blue cones in the macaque retina. *Journal of Neuroscience* **12**, 1233-1252.

LENNIE, P. & D'ZMURA, M. (1988). Mechanisms of color vision. *CRC Critical Review of Neurobiology* **3**, 333-400.

LIVINGSTONE, M.S. & HUBEL, D. (1988). Do the relative mapping densities of magno- and parvocellular systems vary with eccentricity? *Journal of Neuroscience* **8**, 4334-4339.

MARIANI, A.P. (1990). Amacrine cells of the rhesus monkey retina. *Journal of Comparative Neurology* **301**, 382-400.

MARSHAK, D.W., ALDRICH, L.B., DEL VALLE, J. & YAMADA, T. (1990). Localization of immunoreactive cholecystokinin precursor to amacrine cells and bipolar cells. *Journal of Neuroscience* **10**, 3045-3055.

PERRY, V.H. & COWEY, A. (1985). The ganglion cell and cone distributions in the monkey's retina: Implications for central magnification factors. *Vision Research* **25**, 1795-1810.

PERRY, V.H., OEHLER, R. & COWEY, A. (1984). Retinal ganglion cells that project to the dorsal lateral geniculate nucleus in the macaque monkey. *Neuroscience* **12**, 1101-1123.

PETERSEN, M., DACEY, D.M. & ALLEN, K. (1991). Midget and parasol ganglion cells of the human retina. *Investigative Ophthalmology and Visual Science* **32**, 1130.

POLYAK, S.L. (1941). *The Retina*. Chicago, Illinois: University of Chicago Press.

RODIECK, R.W. (1973). *The Vertebrate Retina*. San Francisco, California: W.H. Freeman and Co.

RODIECK, R.W. (1991). Which cells code for color? In *From Pigments to Perception*, ed. VALBERG, A. & LEE, B.B., pp. 83-94. New York: Plenum Press.

RODIECK, R.W., BINMOELLER, K.F. & DINEEN, J. (1985). Parasol and midget ganglion cells of the human retina. *Journal of Comparative Neurology* **233**, 115-132.

RODIECK, R.W., DACEY, D.M. & WATANABE, M. (1987). Some other ganglion cell types of the primate retina. *Investigative Ophthalmology and Visual Science* (Suppl.) **28**, 261.

RODIECK, R.W. & WATANABE, M. (1988). Morphology of ganglion cells that project to the parvocellular laminae of the lateral geniculate nucleus, pretectum, and superior colliculus. *Society of Neuroscience Abstract* **14**, 1120.

SCHEIN, S.J. & DE MONASTERIO, F.M. (1987). Mapping of retinal and geniculate neurons onto striate cortex of macaque. *Journal of Neuroscience* **7**, 996-1009.

STRETTOI, E., RAVIOLA, E. & DACHEUX, R.F. (1992). Synaptic connections of the narrow-field bistratified rod amacrine cell (AII) in the rabbit retina. *Journal of Comparative Neurology* **325**, 152-168.

VANEY, D.I. (1985). The morphology and topographic distribution of AII amacrine cells in the cat retina. *Proceedings of the Royal Society B* (London) **224**, 475-488.

VANEY, D.I. (1991). Many diverse types of retinal neurons show tracer coupling when injected with biocytin or Neurobiotin. *Neuroscience Letters* **125**, 187-190.

WÄSSLE, H., GRÜNERT, U., RÖHRENBECK, J. & BOYCOTT, B.B. (1990). Retinal ganglion cell density and cortical magnification factor in the primate. *Vision Research* **30**, 1897–1911.

WÄSSLE, H. & RIEMANN, H.J. (1978). The mosaic of nerve cells in the mammalian retina. *Proceedings of the Royal Society B* (London) **200**, 441–461.

WATANABE, M. & RODIECK, R.W. (1989). Parasol and midget ganglion cells of the primate retina. *Journal of Comparative Neurology* **289**, 434–454.

WIESEL, T.N. & HUBEL, D.H. (1966). Spatial and chromatic interactions in the lateral geniculate body of the rhesus monkey. *Journal of Neurophysiology* **29**, 1115–1156.

ZRENNER, E., ABRAMOV, I., AKITA, M., COWEY, A., LIVINGSTONE, M. & VALBERG, A. (1990). Color Perception. In *Visual Perception: The Neurophysiological Foundations*, ed. SPILLMANN, L. & WERNER, J.S., pp. 163–204. San Diego, California: Academic Press.

ZRENNER, E. & GOURAS, P. (1981). Characteristics of the blue-sensitive cone mechanism in primate retinal ganglion cells. *Vision Research* **21**, 1605–1609.